Journal of Machine Engineering, 2026, Vol. 26
ISSN 1895-7595 (Print) ISSN 2391-8071 (Online)

Received*: 26 February 2026* / Accepted: *13 May 2026* / Published online: *02 June 2026*

additive manufacturing,
laser powder bed fusion,
titanium

Malek ABU-GHARBIEH[1*], Eckart UHLMANN[1,2],
Andreas SCHWITALLA[3], Rafik AKHMAD[3]

QUALIFICATION OF AN ADDITIVE-SUBTRACTIVE PROCESS FOR MEDICAL IMPLANTS VIA POWDER BED FUSION OF COMMERCIALLY PURE TITANIUM USING A LASER BEAM

Additive manufacturing with powder bed fusion of metals using a laser beam (PBF-LB/M) enables the manufacturing of complex medical implant geometries, such as patient-specific dental implants that replicate the shape of natural tooth roots. Such geometries may support improved osseointegration in the jawbone. This study investigates commercially pure titanium grade 2 (TiGd2) produced by PBF-LB/M as the basis of an additive-subtractive process for medical implants. Specimens were manufactured in different build orientations (BO) to assess material and surface properties. Micro computed tomography indicated a low internal defect density. Tensile testing showed BO-dependent anisotropy, whereas compression testing showed no pronounced anisotropy. Across all BO, mean values were ultimate tensile strength R_m = 772 MPa, elongation at break A = 24.4 %, and compressive yield strength R_{dp} = 746 MPa. Surface post-processing enabled adjustment of roughness, with Ra decreasing from Ra_{as} = 6.3 µm in the as-built state to Ra_{pb} = 5.1 µm after particle blasting, Ra_{et} = 3.6 µm after acid etching, and Ra_{df} = 0.36 µm after disc finishing. Overall, the results confirm the potential of PBF-LB/M-processed TiGd2 for additive-subtractive manufacturing of medical implants.

1. INTRODUCTION

In medical engineering, implants are utilised to restore or support biological functions. In dentistry, for instance, dental implants serve as artificial roots to securely attach various types of prosthetic restorations to the jawbone. Existing implants are limited in their adaptability to anatomical conditions, in terms of osseointegration, defined as the contact between bone tissue and implant, and in service life [1]. Additive manufacturing (AM) allows medical implant geometries tailored to specific load cases and supports improved osseointegration. In the dental context, this can be achieved through patient-specific implant

[1] Institute for Machine Tools and Factory Management, Technische Universität Berlin, Germany
[2] IPK, Fraunhofer Institute for Production Systems and Design Technology, Germany
[3] Department of Prosthodontics, Geriatric Dentistry and Craniomandibular Disorders, Charite – Universitätsmedizin Berlin, Germany
[*] E-mail: abu-gharbieh@tu-berlin.de
https://doi.org/10.36897/jme/221789

geometries that match the shape of natural tooth roots, also known as root analogue implants [1]. AM of metallic implants is often carried out by powder bed fusion of metals using a laser beam (PBF-LB/M). In this process, metallic powder is selectively melted layer by layer [2]. Titanium is frequently used in medical implants due to its biocompatibility and corrosion resistance. In particular, its high tensile strength contributes to the functionality and longevity of implants [3]. Although the titanium alloy Ti6Al4V is widely used for implants, the alloying elements aluminum and vanadium are suspected of being carcinogenic and potentially associated with Alzheimer's disease [4]. Commercially pure titanium (cp-Ti) grades such as titanium grade 2, grade 3 and grade 4 with a purity of 98.0 % ≤ RT ≤ 99.6 % are therefore preferred for implants [3]. While this study is aimed at dental implants as its use case, the resulting findings remain applicable to a broad range of cp-Ti components in medical and industrial engineering.

In AM, BO, process parameters and post-processing can significantly influence both mechanical properties and surface topography [5]. The surface characteristics directly affect osseointegration, therefore the investigation of relevant post-processing is required [6]. For additively manufactured *cp-Ti* only a few coherent datasets are available and compared with conventionally manufactured materials. Differences are often observed in surface structure, microstructure and mechanical strength [7].

Current research efforts aim to develop a software-assisted additive-subtractive manufacturing approach for patient-specific dental implants, as outlined by Abu-Gharbieh et al. [8]. PBF-LB/M is often used to achieve near-net-shape parts, but functional features with tight tolerances such as fits or interfaces are in practice often produced by subsequent conventional machining [9]. A sound qualification of the additive process is therefore a prerequisite for reproducible material and surface properties. Accordingly, the objective of this work was a comprehensive characterisation and qualification of the AM process for titanium grade 2 (TiGd2). Possible internal defects are analysed by micro computed tomography (µCT). The mechanical properties are investigated by tensile and compression tests in different BO to capture potential anisotropy. In addition, the microstructure was characterised using scanning electron microscopy (SEM). Surface characterisation is performed on additively manufactured specimens in several post-processing conditions by tactile roughness measurements and SEM imaging. Finally, the results are compared with values reported in the literature for additively and conventionally manufactured *cp-Ti*.

2. MATERIAL AND METHODS

For the manufacturing of the specimen geometries, a PBF-LB/M system of type SLM 250 HL, NIKON SLM SOLUTIONS AG, Lübeck, Germany, was used. The system is equipped with a single laser with a maximum laser power of P_l = 400 W. A build volume reduction module was used, resulting in a build volume of L × W × H = 150 mm × 150 mm × 150 mm. TiGd2 powder with a particle size of 15 µm ≤ p_s ≤ 45 µm, ECKART GMBH, Hartenstein, Germany, was used. The build chamber was preheated to a temperature of T_h = 200°C. Argon was used as an inert gas and a stripe scanning strategy was applied. A layer thickness of s = 50 µm and a hatch spacing of h = 120 µm were applied. A laser power

of P = 250 W and a scan speed of v_s = 975 mm/s were set, corresponding to a volumetric energy density of $E_v \approx 43$ J/mm³. The specimen geometries investigated in this work are shown in Fig. 1. The arrow indicates the build direction (BD). The BO denotes the angle between the longitudinal axis of the specimen and the plane of the build plate.

Rectangular specimens with a length of L = 10 mm, a width of w = 4 mm and a thickness of t = 2 mm, as shown in Fig. 1a, were analysed by µCT. Measurements were performed on a Metrotom 800, CARL ZEISS INDUSTRIELLE MESSTECHNIK GMBH, Oberkochen, Germany. A voxel size of v_{voxel} = 8.69 µm was used. The tube voltage of U = 130 kV and the tube current of I = 62 µA were applied. In total, 1,450 projections were acquired with an integration time of t_{int} = 667 ms per projection. To reduce beam hardening, an aluminium prefilter with a thickness of d_{pre} = 0.5 mm was used. Data evaluation was carried out with myVGL 2022, HEXAGON AB, Stockholm, Sweden. In addition, specimen volume and part density were determined using the Archimedes method according to DIN EN ISO 3369:2010 and compared with the µCT results. A precision scale PLS 1200 3A, KERN & SOHN GMBH, Balingen, Germany, was used with high purity isopropanol as the medium. For the calculation of relative density, a bulk density of ρ_{abs} = 4.5 g/cm³ for TiGd2 was assumed [10].

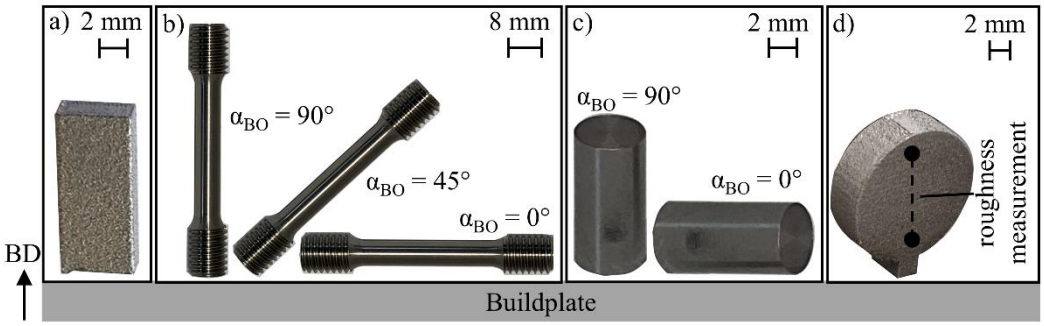

Fig. 1. Specimen overview with BD and BO indicated; a) µCT specimens; b) tensile specimens; c) compression specimens; d) specimen for surface topography measurement

To investigate the mechanical properties of TiGd2 tensile tests were performed according to DIN EN ISO 6892-1 and compression tests according to DIN 50106. Specimens were built at α_{BO} = 0° and α_{BO} = 90° relative to the build plate as shown in Fig. 1b and Fig. 1c. In addition, tensile specimens were built at α_{BO} = 45°. To ensure statistically meaningful results, three specimens per group were tested. The specimens were placed randomly on the build plate and oriented at 30° to the powder recoater. Separation from the build plate was carried out by wire electrical discharge machining (EDM). Final geometries were achieved by turning. The cylindrical compression specimens had diameter d_{ca} = 5 mm and height h_{ca} = 11 mm in the as-built state and diameter d_{c0} = 4 mm and height h_{c0} = 8 mm in the as-machined state. Tensile specimens measured d_{ta} = 8.5 mm in diameter and L_{ta} = 62 mm in length in the as-built state. After machining, a specimen geometry according to DIN 50125, form B, with M8 threads was used, with a parallel section diameter $d0$ = 5 mm, an initial gauge length $L0$ = 25 mm, and a total length LT = 51 mm.

Mechanical testing was performed on a universal testing machine Z150, ZWICKROELL GMBH & CO. KG, Ulm, Germany, at room temperature. The tensile test strain was measured using an extensometer macroXtens II, ZWICKROELL GMBH &

CO. KG, Ulm, Germany. The test speed in the elastic range was v_E = 1.4 µm/s and in the plastic range v_R = 40 µm/s. For the compression tests, strain was calculated from the crosshead displacement. The compression test speed was v_C = 52 µm/s.

Microstructure and chemical analysis were carried out externally by TANIOBIS GMBH, Goslar, Germany. The microstructural analysis was performed at a magnification M = 200 using a scanning electron microscope JSM 7200F, JEOL LTD., Tokyo, Japan. Samples were taken from the threaded regions of tensile specimens, with one specimen built at α_{BO} = 0° and one built at α_{BO} = 90°. The threaded sections were cut at mid thread, cold-mounted in epoxy resin, and ground to a final abrasive size of s_a = 10 µm. The specimens were then polished for t = 10 min using an oxide polishing suspension OP-S, STRUERS APS, Ballerup, Denmark. The chemical compositions were determined at the same laboratory by inductively coupled plasma optical emission spectroscopy using a PlasmaQuant PQ 9000/9100, ANALYTIK JENA GMBH, Jena, Germany, and carrier gas hot extraction and combustion analysis using TCH-600 and ONH-836 as well as CS-744, LECO CORPORATION, St. Joseph, USA.

For surface characterisation and the investigation of the post-processing, cylindrical specimens with diameter d = 12.5 mm and thickness h = 4 mm were manufactured, as shown in Fig. 1d. This specific geometry was selected for surface characterisation to ensure direct compatibility with the specimens intended for subsequent in vitro tests according to DIN EN ISO 10993. The specimens were built with the cylinder axis parallel to the build plate in order to align the cylindrical lateral surface parallel to the BD. The specimen surfaces were examined in the as-built condition and after processing by particle blasting, acid etching and disc finishing. For each post-processing condition three specimens were examined. On each specimen the two opposite lateral surfaces were measured once, so that the mean value was determined from a total of six roughness measurements per condition.

Particle blasting was performed using an HGH 7050 DUO, HGH VERTRIEBS GMBH, Lüdenscheid, Germany, with blasting media corundum F90. The parameters were blasting pressure of p_b = 7 bar, blasting distance of x_b = 30 mm and a processing time per specimen of t_b = 3 min. The specimens that were subsequently processed using disc finishing or acid etching were blasted beforehand as a pretreatment, using the above parameters. During acid etching the blasted specimens were treated in a solution of water (H_2O), hydrofluoric acid (HF) and hydrogen peroxide (H_2O_2) with a ratio H_2O:HF:H_2O_2 = 3:1:6. The specimens were placed in a chemically resistant container, and the solution was added until the specimens were fully covered. After an etching time of t_e = 12 min the specimens were removed, rinsed in water and then cleaned in an ultrasonic bath with ethanol for t_r = 10 min. The disc-finished specimens were post-processed on a centrifugal disc finishing machine Eco Maxi, OTEC PRÄZISIONSFINISH GMBH, Straubenhardt, Germany. Disc finishing was performed in two steps. Coarse grinding used ceramic abrasive media at a disc speed of n = 280 rpm for a processing time of t_{cg} = 3 h. Fine grinding used plastic bonded media at the same disc speed of n = 280 rpm for a processing time of t_{fg} = 2 h.

For qualitative surface characterisation, SEM was performed using a Phenom XL, THERMO FISHER SCIENTIFIC EINDHOVEN B.V., Eindhoven, Netherlands. Images were acquired at magnification of M = 250 and accelerating voltage of U = 15 kV. Backscattered electron images (BSE) were recorded. Roughness measurements were carried

out using a Surftest SJ 410, MITUTOYO CORPORATION, Kawasaki, Japan, at cut-off wavelength of λ = 2.5 mm, evaluation length of l_m = 5 mm and tip radius of r_t = 5 µm. Measurements were performed on the lateral surfaces of the specimen, as shown in Fig. 1d.

3. RESULTS

In Fig. 2, the results of the µCT analysis are presented. Fig. 2a shows the rectangular specimen as a three-dimensional reconstruction with colour-coded defects, where the colour indicates the defect diameter. Most defects are located at the external surface, where the largest defect diameters are also observed. A possible reason is the rough surface topography typical of PBF-LB/M, which may be caused by adhering or partially melted powder particles and may lead to a high number of detected defects in this region. Fig. 2b shows a cross-section through the specimen volume, indicating that only a few defects occur in the interior. Most interior defects have diameters below d_D = 0.1 mm. The red arrows highlight defects located close to the outer surface. These defects could be related to unsuitable contour or hatch spacing parameters and may be mitigated by adjusting these parameters. Fig. 2c shows a detail from the specimen interior containing the largest detectable defect of $d_D \approx 0.1$ mm, which could correspond to a gas or a keyhole-induced pore. Overall, the µCT results indicate a low defect density in the interior, while most defects occur in the subsurface region and could be removed by appropriate post-processing.

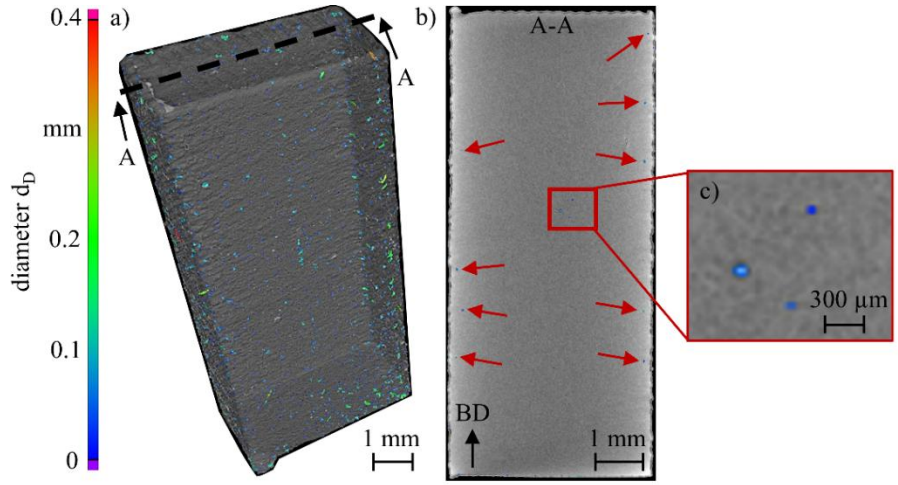

Fig. 2. µCT analysis of a rectangular specimen; a) three-dimensional rendering with colour-coded defect diameter; b) section A-A showing internal defects; c) detail view of larger defects

Based on the µCT data, the specimen volume V_{CT} = 78.47 mm³ and the resulting relative density $\rho_{rel,CT}$ = 99.95 % were determined and compared with the Archimedes measurement. The Archimedes measurement yielded a volume of V_A = 76.51 mm³ and a relative density of $\rho_{rel,A}$ = 99.88 %. Thus, the µCT analysis resulted in a slightly larger volume and a higher relative density. Both methods indicate a high relative density of the specimens and therefore a low internal porosity.

3.1. TENSILE TEST

The results of the tensile tests are shown as stress–strain curves in Fig. 3. After an initially similar response in the elastic region, the curves diverge after yielding. Specimens built at $\alpha_{BO} = 0$ exhibit a higher stress level in the plastic region and reach the maximum stress at a lower tensile strain, indicating earlier necking, which is consistent with the reduced elongation at break. Table 1 presents the mean values of the derived properties and their standard deviation. The properties at $\alpha_{BO} = 90°$ and $\alpha_{BO} = 45°$ differ only slightly. In contrast, specimens built at $\alpha_{BO} = 0°$ exhibit higher yield strength (YS) $R_{p0.2}$, ultimate tensile strength (UTS) R_m, and Young's modulus (YM) E. At the same time, the elongation at break (EAB) A is lower at $\alpha_{BO} = 0°$, which may indicate a less ductile and therefore more brittle material response compared with $\alpha_{BO} = 90°$ and $\alpha_{BO} = 45°$.

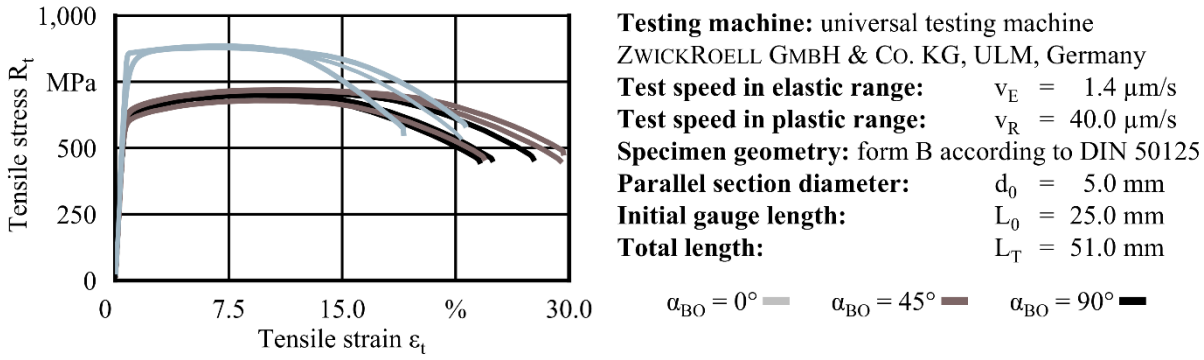

Fig. 3. Stress–strain curves of tensile testing for specimens built at $\alpha_{BO} = 0°$, $\alpha_{BO} = 45°$ and $\alpha_{BO} = 90°$

One possible reason is a difference in microstructure. The layer-by-layer build process and the directional heat flow promote preferred grain growth along the BD and a directional arrangement of microstructural features. As a result, plastic flow and deformation behaviour may be anisotropic with respect to the loading direction [11]. This interpretation is supported by the SEM images of the tensile specimens shown in Fig. 4. Fig. 4a shows a cross-section parallel to the BD. The microstructure exhibits elongated features that are preferentially aligned with the BD, indicating a directional microstructural arrangement. Fig. 4b shows a cross-section perpendicular to BD. The microstructure appears more colony-like, and the lamellar features are less uniformly oriented within the image plane. In both images, no coarse inclusions, pores, or microcracks are visible within the field of view, suggesting that suitable PBF-LB/M process parameters were used. This comparison is consistent with findings reported in the literature, such as those by Cao et al. for PBF-LB/M of Ti-6Al-4V [11].

Table 1. Mechanical properties derived from tensile tests: yield strength (YS) $R_{p0.2}$, ultimate tensile strength (UTS) R_M, Young's modulus (YM) E and elongation at break (EAB) A reported as mean values with standard deviation in brackets

Property	-	$\alpha_{BO} = 90°$	$\alpha_{BO} = 45°$	$\alpha_{BO} = 0°$
YS $R_{p0.2}$	MPa	608.4 (8.1)	614.7 (15.1)	796.8 (45.6)
UTS R_m	MPa	714.8 (6.4)	715.0 (19.5)	887.3 (2.7)
YM E	GPa	109.2 (3.9)	113.8 (4.9)	115.6 (1.5)
EAB A	1	25.5 (1.5)	25.9 (2.5)	21.7 (1.8)

The differences in tensile test results between BO may also be related to the chemical composition of the specimens. The mass fractions of carbon, hydrogen, nitrogen, and oxygen are given in Table 2. "Max" denotes the maximum permissible content in the powder for TiGd2, "Powder" the values reported by the powder manufacturer ECKART GMBH, Hartenstein, Germany, "$\alpha_{BO} = 0°$" and "$\alpha_{BO} = 90°$" the values determined by TANIOBIS GMBH, Goslar, Germany, as described in Section 2. The aim was to assess how the chemical composition of the powder compares with that of the additively manufactured specimens. To this end, the measured values were compared with the powder manufacturer's specification. For nitrogen, the specimen values were $w_{N,0°} = 235.6$ ppm and $w_{N,90°} = 133.3$ ppm. These values are higher than the powder value $w_{N,p} = 30.0$ ppm but remain below the maximum permissible value $w_{N,max} = 300.0$ ppm. Carbon and hydrogen did not show any significant deviation between powder and specimens. The oxygen content was higher in both specimens than in the powder but remained below the maximum permissible value $w_{O,max} = 2{,}500$ ppm.

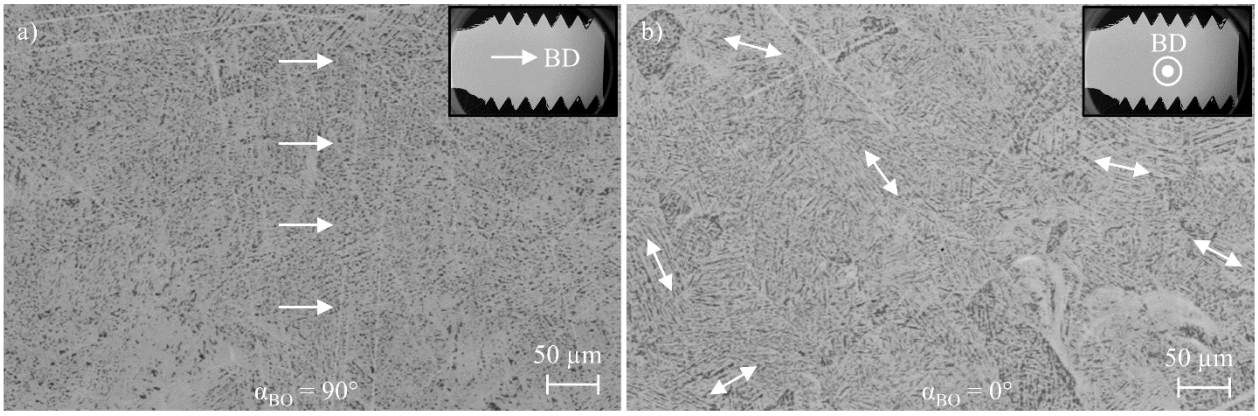

Fig. 4. SEM images of cross sections of tensile specimens; a) $\alpha_{BO} = 90°$ white arrows indicate the alignment of the microstructure with the BD; b) $\alpha_{BO} = 0°$ white arrows highlight locally varying orientations of lamellar features within the image plane; SEM images recorded by TANIOBIS GmbH, Goslar, Germany

Specimens built at $\alpha_{BO} = 0°$ showed an increase in nitrogen content of 77 % and an increase in oxygen content of 44 % compared to those built at $\alpha_{BO} = 90°$. This enrichment can be attributed to the thermal conditions during the PBF-LB/M process. The larger cross-sectional areas and longer scan tracks of the $\alpha_{BO} = 0°$ specimens promote heat accumulation, leading to prolonged periods at elevated temperatures at which titanium is highly reactive [12]. Both oxygen and nitrogen act as interstitial strengtheners, where nitrogen is known to have a significantly higher strengthening potency than oxygen [13]. Therefore, the enrichment of both elements, with nitrogen playing the dominant role, provides an explanation for the superior strength and reduced EAB observed in the $\alpha_{BO} = 0°$ specimens.

Table 2. Results of the chemical analysis

Type	-	N	C	H	O
Max	ppm	300.0	800.0	150.0	2,500
Powder	ppm	30.0	200.0	20.00	1,400
$\alpha_{BO} = 0°$	ppm	235.6	123.1	20.13	2,125
$\alpha_{BO} = 90°$	ppm	133.3	123.1	20.10	1,472

3.2. COMPRESSION TEST

During compression testing, all specimens exhibited ductile deformation without fracture, as shown in Fig. 5. Therefore, the tests were conducted up to a compressive strain of ε_c = 50 %. For specimens built at α_{BO} = 90°, the compressive stress at 50 % strain (CS50) was R_{dm50} = 2,320 ± 96 MPa and the compressive yield strength (CYS) was $R_{dp0.2}$ = 760 ± 25 MPa. For specimens built at α_{BO} = 0°, values of R_{dm50} = 2,208 ± 59 MPa and $R_{dp0.2}$ = 732 ± 17 MPa were obtained. The values for α_{BO} = 90° were slightly higher than those for α_{BO} = 0°. However, the difference is small and may be within the standard deviation of the measurements. Accordingly, the compression tests do not indicate an anisotropy with respect to BO. The observed trends suggest that specimen orientation may have a stronger influence on deformation and failure in tension than in compression. This may be related to the different loading modes. Under compressive loading, layer-parallel irregularities and pores may tend to close, which can make potential crack initiation sites less effective [14].

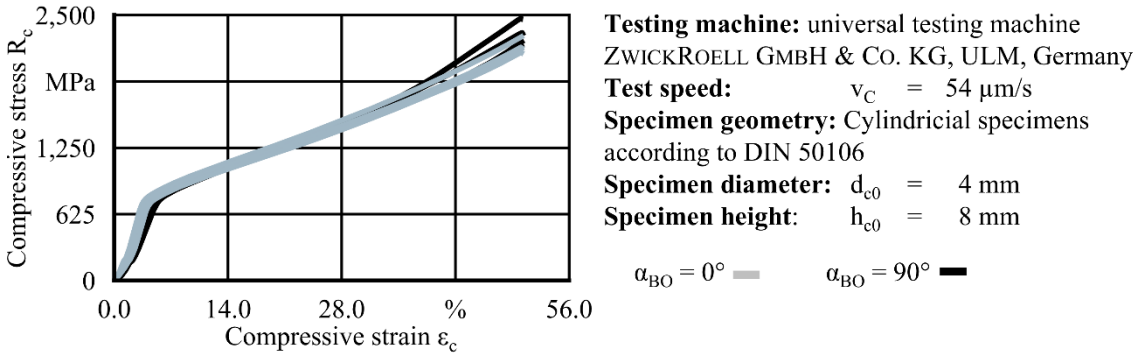

Fig. 5. Stress-strain curves from compression tests for specimens built at α_{BO} = 0° and α_{BO} = 90°

3.3. POST-PROCESSING

The SEM images of specimen surfaces are shown in Fig. 6 and the Arithmetic mean height (AMH) *Ra* and Maximum height (MH) *Rz* obtained from the surface measurements are shown in Table 3.

As described in Section 2, the lateral surfaces of the specimens were examined. The as-built specimens shown in Fig. 6a exhibit the surface topography typical of PBF-LB/M, with a AMH of Ra_{as} = 6.3 µm. Melt tracks and partially remelted powder particles are visible. The particle blasted specimens in Fig. 6b exhibit a more homogeneous topography. Particle adhesions are reduced and roughness peaks are diminished, resulting in a AMH of Ra_{pb} = 5.1 µm. Pronounced melt tracks are no longer visible. Fig. 6c shows the acid-etched specimens. The surface is smoothed while remaining finely structured, with a AMH of Ra_{et} = 3.6 µm. Such microstructured surfaces are considered favourable for implant applications because cell attachment may be promoted [6]. In contrast, the disc-finished specimens in Fig. 6d show a uniform, strongly smoothed surface with a AMH of Ra_{df} = 0.36 µm. Overall, the post-processing routes demonstrate that distinct topographies with varying roughness values can be achieved depending on the applied process step.

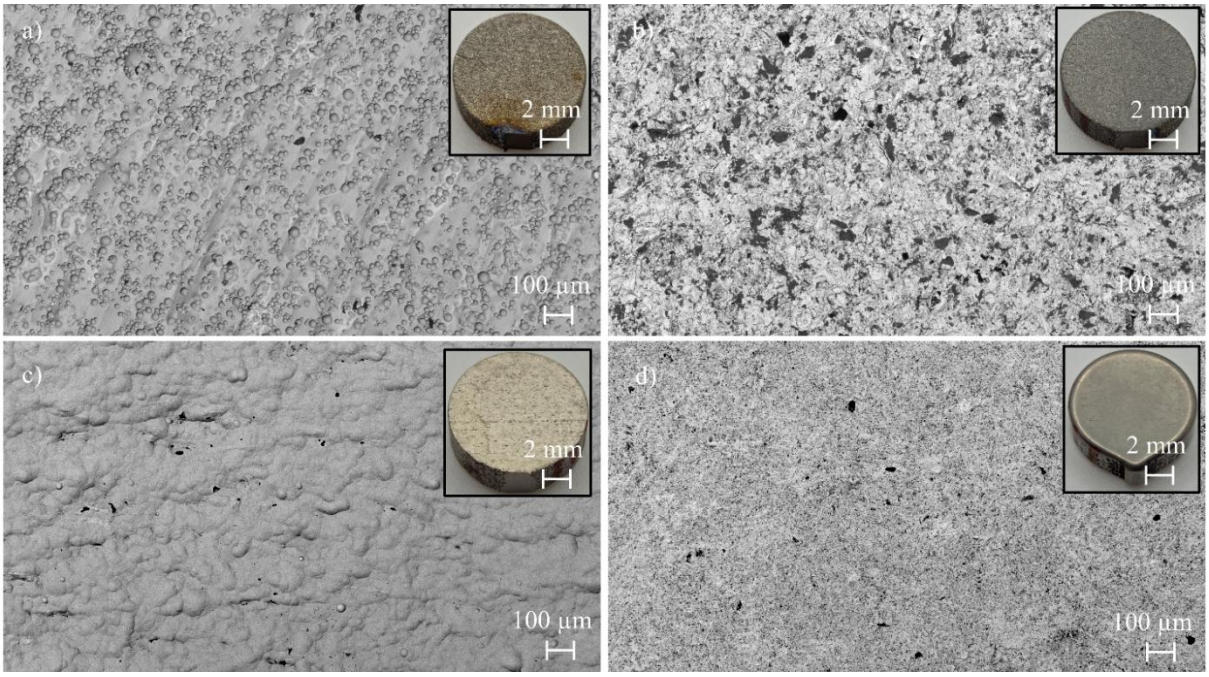

Fig. 6. SEM images of specimen surfaces in different post-processing conditions with corresponding specimen image shown in each panel; a) as-built; b) particle blasting; c) acid etching; d) disc finishing

Table 3. Tactile roughness measurements of the different surface conditions reported as mean values with standard deviation in brackets

Condition	-	AMH Ra	MH Rz
As-built	µm	6.27 (0.30)	44.1 (3.01)
Particle blasting	µm	5.08 (0.21)	37.9 (3.70)
Acid etching	µm	3.60 (0.41)	29.3 (2.78)
Disc finishing	µm	0.36 (0.10)	7.5 (2.13)

4. DISCUSSION

In Table 4, the values determined in this study from tensile and compression tests as well as from roughness measurements of the as-built specimens are summarised. To place the results in context, values obtained at different BO are reported as an overall mean value. In addition, literature data for additively manufactured cp-Ti produced by PBF-LB/M and reference values for conventionally manufactured (CM) TiGd2 are included.

A comparison with literature reports was used to assess the plausibility of the results. Haase et al. report tensile results for titanium Grade 1 (TiGd1) in a similar range [15]. For TiGd1, lower strength would generally be expected, since TiGd1 typically contains fewer interstitial elements, in particular oxygen, than TiGd2. Haase et al. show, that the oxygen, nitrogen, and hydrogen contents increased compared with the powder specification. The measured oxygen contents exceed the limits for TiGd1 and approach those for TiGd2. This may explain why the mechanical properties are comparable despite the different grade. Overall, this underlines the need to verify the chemical composition of the built material for additively manufactured materials, since it can change during the AM process. Furthermore,

only a few publications report compressive properties of cp-Ti produced by PBF-LB/M. Attar et al. report distinctly lower values [7]. The CYS R_{dp} is approximately 43 % lower than the value determined in this work. A possible reason is a different part quality caused by varying process parameters. Attar et al. report a relative density of ρ_{rel} = 99.5 %, whereas relative densities around ρ_{rel} = 99.9 % were achieved in this study [7]. It is therefore plausible that the density increase achieved in this study is related to the lower defect content.

When comparing tensile test values obtained in this study with reference values for CM TiGd2, taken from a data sheet provided by ASM Aerospace Specification Metals Inc., Florida, USA, the additively manufactured specimens show markedly higher YS and UTS, while YM and EAB show slightly higher values [17]. In this study, the YS of $R_{p0.2}$ = 673 MPa is approximately 96 % higher than the data sheet value of $R_{p0.2}$ = 344 MPa. For the UTS, R_m = 772 MPa is approximately 88 % higher than the upper data sheet value of R_m = 410 MPa. A possible reason for the observed differences may be attributed to thermal process conditions. CM cp-Ti is typically supplied as a semi-finished product manufactured by casting followed by forming and heat treatment [7]. In PBF-LB/M, the high heating and cooling rates can lead to fine microstructure that differs from the comparatively coarse microstructure of CM parts [7]. A finer microstructure increases the density of microstructural boundaries, which hinders dislocation motion during plastic deformation. As a result, the stress required for the onset of plastic flow increases, and higher strength values are typically obtained [18].

Overall, the investigations show that the TiGd2 specimens produced by PBF-LB/M achieve higher strength values compared to CM TiGd2. The results provide key data for the design of subsequent process steps, in particular for the selection of suitable tools and process parameters for conventional finishing.

When comparing the roughness values measured in this study for the as-built specimens of Ra = 6.3 ± 0.3 µm and Rz = 44 ± 3 µm with values reported in the literature, Petrusa et al. report a higher AMH of Ra = 7.5 ± 0.5 µm and a slightly lower MH of Rz = 40 ± 5 µm for TiGd2 [16]. These comparatively low roughness values, reported in this study suggest that a uniform surface with limited particle adhesion was achieved, which can be taken as an indication of suitable process parameters. At the same time, the comparatively high AMH value relative to MH indicates that isolated roughness peaks may still be present.

In the context of patient-specific dental implants, different functional regions of a medical device may require distinct surface topographies because they interface with different tissues and cell populations. Areas intended for bone contact often benefit from a defined micro-roughness to support osseointegration. In contrast, regions interacting with soft tissue may require different topographical characteristics. Functional fit surfaces or regions with tight dimensional tolerances typically require smoother finishes to ensure accurate seating. Based on this, the investigated post-processing conditions can be regarded as selectable modules within a process chain, enabling region specific tailoring of the surface according to local functional and biological demands [6].

Particle blasting reduces adhered powder particles and homogenizes the as-built surface. It is an effective step for cleaning and for reducing pronounced roughness peaks. In addition, particle blasting can serve as a pre-treatment for subsequent post-processing by removing loosely bound particles and residues, so downstream processes such as acid etching or disc

finishing start from a more uniform initial surface. Thus, process efficiency may be enhanced while reproducibility is improved. Acid etching further reduces roughness while generating a finely structured surface that may support cellular attachment. When particle blasting is combined with subsequent acid etching, a three-dimensional hierarchical topography can be achieved. Particle blasting introduces microscale roughness, while acid etching superimposes nanoscale features, resulting in a multiscale surface architecture [6]. In contrast, disc finishing primarily smoothest the surface and yields the lowest roughness values. It is therefore particularly suitable for contact areas exposed to the oral environment, where a smoother surface may help limit bacterial adhesion.

Overall, the results support the assessment that PBF-LB/M of TiGd2 in combination with suitable surface post-processing provides a viable process window to adjust function relevant properties for patient-specific dental implants. Planned in vitro studies will evaluate the suitability of the investigated surface conditions for the intended application. In addition, the material properties determined in this work together with the results on defects and surface characterisation provide a basis for subsequent process steps. Future work should therefore examine the transfer of the results to complex implant geometries.

Table 4. Comparison of measured properties of PBF-LB/M TiGd2 with literature values and conventionally manufactured (CM) TiGd2 with standard deviation in brackets

Property	-	PBF-LB/M [This study]	PBF-LB/M [7, 15, 16]	CM [17]
YS $R_{p0.2}$	MPa	673 (92)	639 - 676	344
UTS R_m	MPa	772 (82)	723 - 767	275 - 410
YM E	GPa	113 (5)	108 - 125	105
EAB A	1	24 (3) %	24 - 27 %	20
CYS R_{dp}	MPa	746 (7)	427 (7)	-
CS50 R_{dm50}	MPa	2248 (92)	1046 (16)	-
AMH Ra	µm	6.3 (0.3)	7.5 (0.5)	-
MH Rz	µm	44.0 (3.0)	40.0 (5.0)	-

5. SUMMARY

This study investigated additively manufactured TiGd2 using PBF-LB/M and characterised defects, mechanical properties, microstructure, chemical composition, and surface post-processing. The µCT analysis indicated a low internal defect density, with most defects located near the subsurface region. The relative density was $\rho_{rel,CT}$ = 99.95 % from µCT and $\rho_{rel,A}$ = 99.88 % from the Archimedes method. Tensile testing showed a pronounced dependence on BO, where specimens built at α_{BO} = 0° exhibited higher YS $Rp_{0.2}$, UTS R_m, and YM E, while the EAB A was lower compared with α_{BO} = 90° and α_{BO} = 45°. Compression testing showed ductile deformation without fracture up to 50 % strain and only minor differences between orientations. Across all BO tested, the mean mechanical properties were YS of $R_{p0.2}$ = 673 ± 92 MPa, UTS of R_m = 772 ± 82 MPa, YM of E = 113 ± 4.6 GPa, EAB of A = 24.4 ± 2.8 %, CS50 of R_{dm50} = 2248 ± 92 MPa and CYS of $R_{dp0.2}$ = 746 ± 7.1 MPa. Furthermore, SEM revealed a directional microstructural arrangement aligned with the BD,

supporting the observed anisotropy in tension. The oxygen and nitrogen contents were higher in both BO than in the powder state but remained below the maximum permissible values. The increased interstitial contents may contribute to the higher strength through interstitial strengthening. Surface post-processing enabled different surface topographies and roughness levels. The surface roughness of the as-built specimens was Ra_{as} = 6.3 µm and decreased to Ra_{pb} = 5.1 µm after particle blasting, Ra_{et} = 3.6 µm after acid etching, and Ra_{df} = 0.36 µm after disc finishing. In summary, the characterisation presented in this study indicates that TiGd2 can be manufactured by PBF-LB/M with low internal defect density, high mechanical properties and different surface conditions, which supports the qualification of the additive process prior to subsequent machining.

ACKNOWLEDGEMENTS

This publication is based on results from the ProFIT collaborative project "ProAStra Dental", which received financial support from the European Union through the European Regional Development Fund (ERDF). The research project was carried out in collaboration with TRINCKLE GMBH, Berlin, Germany.
Furthermore, the authors thank TANIOBIS GMBH, Goslar, Germany, for metallographic specimen preparation, SEM imaging and elemental analyses.

REFERENCES

[1] JIANYU C., ZHIGUANG Z., XIANSHUAI C., XIAO Z., 2017, *Influence of Custom-Made Implant Designs on the Biomechanical Performance for the Case of Immediate Post-Extraction Placement in the Maxillary Esthetic Zone: a Finite Element Analysis*, Computer Methods in Biomechanics and Biomedical Engineering 20/6, 636–644.
[2] UHLMANN, E., PASTL, R., LAGHMOUCHI, H., BERGMANN, A., 2017, *Intelligent Pattern Recognition of a SLM Machine Process and Sensor Data*, Journal of Machine Engineering, 17/2, 65–76.
[3] SILVA, R.C.S., AGRELLI, A., ANDRADE, A.N., MENDES-MARQUES, C.L., ARRUDA, I.R.S., SANTOS, L.R.L., VASCONCELOS, N.F., MACHADO, G., 2022, *Titanium Dental Implants: an Overview of Applied Nanobiotechnology to Improve Biocompatibility and Prevent Infections*, Materials (Basel, Switzerland) 15/9.
[4] HAASE, F., SIEMERS, C., KLINGE, L., LU, C., LANG, P., LEDERER, S., KÖNIG, T., RÖSLER, J., 2020, *Aluminum-And Vanadium-Free Titanium Alloys for Medical Applications*, MATEC Web of Conferences 321 (05008).
[5] UHLMANN, E., BERGMANN, A., JOHN, P., KASHEVKO, V., 2014, *Verification of Design Rules for Additive Manufacturing: Proceedings of Dimensional Accuracy and Surface Finish in Additive Manufacturing*, ASPE, 19–23.
[6] SUBRAMANI, K., MATHEW, R.T., 2012, *Chapter 6 - Titanium Surface Modification Techniques for Dental Implants-from Microscale to Nanoscale*, Subramani, K., Ahmed, W. (Eds.), Emerging Nanotechnologies in Dentistry: Micro and Nano Technologies, William Andrew Publishing, Boston, 85–102.
[7] ATTAR H., EHTEMAM-HAGHIGHI S., KENT D., WU X., DARGUSCH M., 2017, *Comparative Study of Commercially Pure Titanium Produced by Laser Engineered Net Shaping, Selective Laser Melting and Casting Processes*, Materials Science and Engineering: A, 705.
[8] ABU-GHARBIEH M., BRAUN T., SCHWITALLA A., AKHMAD R., FRIEß F., BARVINSKA V., UHLMANN E., 2024, *Additive Fertigung Von Zahnimplantaten,* Entwicklung Einer Innovativen Additiv-Subtraktiven Prozesskette Für Die Zahnmedizin Mittels Laser Powder Bed Fusion-Verfahren, 119/7–8, 539–542.
[9] MOEHRING H.-C., MAUCHER C., BECKER D., STEHLE T., EISSELER R., 2023, *The Additive-Subtractive Process Chain - a Review*, Journal of Machine Engineering, 23/1, 5–35.
[10] OSMAN R.B., SWAIN M.V., 2015, *A Critical Review of Dental Implant Materials with an Emphasis on Titanium Versus Zirconia,* Materials (Basel, Switzerland), 8/3, 932–958.

[11] SHENG C., YICHAO Z., CHAO VOON SAMUEL L., XINHUA W., 2021, *Review of Laser Powder Bed Fusion (LPBF) Fabricated Ti-6Al-4V: Process, Post-Process Treatment, Microstructure, and Property*, Light: Advanced Manufacturing, 2/3.

[12] PAUZON C., DIETRICH K., FORT P., HRYHA E., WITT G., 2021, *Mitigating Oxygen Pick-Up During Laser Powder Bed Fusion of Ti-6Al-4V By Limiting Heat Accumulation*, Materials Letters, 288, 129365.

[13] LEYENS C., PETERS M., 2003, *Titanium and Titanium Alloys: Fundamentals and Applications*, Wiley-VCH, Weinheim, Germany, 1, 36.

[14] DENG X., PIOTROWSKI G.B., WILLIAMS J.J., CHAWLA N., 2005, *Effect of Porosity and Tension-Compression Asymmetry on the Bauschinger Effect in Porous Sintered Steels*, International Journal of Fatigue, 27/10, 1233–1243.

[15] HAASE F., SIEMERS C., RÖSLER J., 2023, *Laser Powder Bed Fusion (LPBF) of Commercially Pure Titanium and Alloy Development for The LPBF Process*, Frontiers in bioengineering and biotechnology, 11, 1260925.

[16] PETRUSA J., MEIER B., GRÜNBACHER G., WALDHAUSER W., ECKERT J., 2022, *Surface Topography and Biocompatibility of Cp-Ti Grade2 Fabricated by Laser-Based Powder Bed Fusion: Influence of Printing Orientation and Surface Treatments*, Advanced Engineering Materials, 25.

[17] *ASM Aerospace Specification Metals*, 2026, Titanium Grade 2: data sheet, ASM Aerospace Specification Metals. https://www.aerospacemetals.com/wp-content/uploads/2023/07/Titanium-Grade-2-Data-Sheet.pdf.

[18] LI D., FAN G., HUANG X., JUUL JENSEN D., MIAO K., XU C., GENG L., ZHANG Y., YU T., 2021, *Enhanced Strength in Pure Ti Via Design of Alternating Coarse- and Fine-Grain Layers*, Acta Materialia, 206, 116627.